electronics

MDPI

Article

Exploring the Functional Brain Network of Deception in Source-Level EEG via Partial Mutual Information

Qianruo Kang, Feng Li and Junfeng Gao *

Key Laboratory of Cognitive Science of State Ethnic Affairs Commission, College of Biomedical Engineering, South-Central Minzu University, Wuhan 430074, China
* Correspondence: 2011040@mail.scuec.edu.cn

Abstract: In this study, partial mutual information at the source level was used to construct brain functional networks in order to examine differences in brain functions between lying and honest responses. The study used independent component analysis and clustering methods to computationally generate source signals from EEG signals recorded from subjects who were lying and those who were being honest. Partial mutual information was calculated between regions of interest (ROIs), and used to construct a functional brain network with ROIs as nodes and partial mutual information values as connections between them. The partial mutual information connections that showed significant differences between the two groups of people were selected as the feature set and classified using a functional connectivity network (FCN) classifier, resulting in an accuracy of 88.5%. Analysis of the brain networks of the lying and honest groups showed that, in the lying state, there was increased informational exchange between the frontal lobe and temporal lobe, and the language motor center of the frontal lobe exchanged more information with other brain regions, suggesting increased working and episodic memory load and the mobilization of more cognitive resources.

Keywords: source reconstruction; partial mutual information; brain network; lie detection

Citation: Kang, Q.; Li, F.; Gao, J. Exploring the Functional Brain Network of Deception in Source-Level EEG via Partial Mutual Information. *Electronics* **2023**, *12*, 1633. https://doi.org/10.3390/electronics12071633

Academic Editors: Ahmed Elnakib, Fahmi Khalifa and Ahmed Soliman

Received: 14 February 2023
Revised: 25 March 2023
Accepted: 28 March 2023
Published: 30 March 2023

1. Introduction

Deception, also known as lying, involves the deliberate dissemination of false information with the intention of influencing the perceptions of others [1]. In the past, much of the research related to this topic has focused on detecting lies, with various physiological indicators such as heart rate, electrodermal response, and respiratory pattern being identified as potential indicators of deception [2]. However, these traditional polygraph techniques have been criticized for their lack of a strong theoretical basis and accuracy concerns [3,4]. In recent years, advances in neuroimaging technology and cognitive neuroscience have allowed for the use of electroencephalography (EEG) [5], functional magnetic resonance imaging (fMRI) [6], and functional near-infrared spectroscopy (fNIRS) [7] to study the brain mechanisms underlying deception. Among these methods, EEG has a higher temporal resolution, making it particularly useful for investigating the neural dynamics of lying. Many researchers have attempted to extract time-frequency domain and phase attributes from EEG signals for analysis. However, these studies often focus on comparing features between single channels and do not take into account the connections between different brain areas [8–10], which may be important for understanding the complex neural processes involved in deception.

Over the past two decades, advances in brain neurodynamics and cognitive neuroscience have led to increased investigation into the neural mechanisms underlying deception. Researchers have utilized functional brain networks to examine the neural basis of lying, and to develop lie detection systems using brain network characteristics [11]. Non-linear analysis techniques, such as graph theory and coherence, have been used to construct functional connection matrices of EEG signals, providing insight into the functional

networks involved in the cognitive processes of deception [12–15]. In addition, mutual information has been utilized to analyze the non-linear synchronization of EEG signals and effectively quantify the transfer of non-linear information between them. These efforts have contributed to a deeper understanding of the neural basis of deception [16,17]. Peng and colleagues developed a lie detection system using brain networks based on mutual information [18]. Their work has shed light on the neural activity and information communication mechanisms in brain areas involved in lying. However, mutual information has been known to produce incorrect lead edges for brain network construction [18]. In an effort to address this issue, Frenzel introduced the use of partial mutual information (PMI) to detect direct coupling between multivariate time series [19]. PMI eliminates indirect coupling, thereby accurately revealing the true coupling structure between the signals [20–22]. Previous research has demonstrated the superiority of PMI in precisely quantifying non-linear direct correlations within networks [23]. Despite these advances, there have been no reported studies on the construction of brain networks using PMI to investigate the cognitive processes of lying.

Many functional connectivity studies using EEG have been conducted using sensor signals, but these signals may be affected by volume conduction, which can hinder the interpretation of connectivity [24,25]. Additionally, the analysis of sensor-based connections does not permit the identification of the specific brain areas involved in functional interactions [26]. These limitations have been noted in previous research. To address the limitations of sensor signals in functional connectivity studies, two types of EEG source reconstruction approaches have been applied to infer the directional connections between brain sources [27–29]. The first method uses a biophysical generative model to infer functional connectivity between sources directly from the sensor data. The second method, which exploits a two-step procedure, is model-free and does not require any network structure assumptions. The first step of the second EEG source reconstruction approach involves the determination of the source signal from sensor-space data using distributed or dipolar source models [30,31], such as minimum norm estimates (MNE), low-resolution electromagnetic tomography (LORETA), and standard low-resolution brain electromagnetic tomography (sLORETA). sLORETA is a variant of the LORETA approach that accounts for both noise variance during EEG measurement and biological variance in the entire brain [32]. Once the source signal has been determined, a functional connection metric is applied to it. This approach has been widely used to infer brain network connections [33]. To study brain connectivity, it is often necessary to divide the brain into ROIs prior to the source estimation process [31,34]. These ROIs can be determined using a pre-defined atlas [35] or a data-driven approach [36,37], such as K-means clustering. This allows for a more detailed analysis of functional connections within the brain.

Phase Lag Index (PLI) [38] and Phase Locking Value (PLV) [39] are both metrics used to measure the phase synchronization properties between two signals. They have been widely used to estimate large-scale neural interactions. In previous research on lie detection using EEG, researchers have utilized phase synchronization to develop a lie detection system [40,41]. This involves constructing a feature vector by applying functional connectivity indicators such as PLV and PLI. The feature vector is then sent to a machine-learning model for classification to build a polygraph system. However, no research is currently available on developing a deception classification system using PMI. This study aims to establish an effective machine learning system based on the PMI method for classification and compare it with two traditional lie detection methods currently in use.

Deception is essentially a complex neuropsychological activity that requires coordination across multiple parts of the brain and involves several cognitive executive skills and control processes [42,43]. In this work, we aim to explore the connectivity and difference analysis of the functional network of lying and construct a high-accuracy lie detection system. To achieve the appeal goal, this research selects the ROI by the K-means clustering method and then employs source reconstruction methods to convert the EEG signal into the source signal. Finally, for the first time, the part mutual information index is used to

build a brain network and lie detection system. In the context of EEG data, PMI can be used to identify pairs of brain regions that show a significant degree of statistical dependence during deception, compared to a control condition (e.g., truth-telling). This can provide insight into the neural mechanisms underlying deception and how it differs from other cognitive processes. The study's novelty can be summed up in three ways:

- To the best of the authors' knowledge, this is the first study to apply partial mutual information to construct a cortical connectivity network from EEG data;
- The PMI adjacency matrix and the brain connectivity graph were used to reveal the interaction between various brain regions' underlying and honest responses;
- This paper explores the performance of different EEG functional connectivity indices in classification steps.

2. Materials and Methods

As shown in Figure 1, the proposed framework consists of seven major steps: EEG recording, data preprocessing, ROI selection, source reconstruction, PMI matrix, PMI connection network, and FCN classification. In this study, the first step involved recording the raw EEG data from the subjects. After thorough preprocessing and analysis, the next step was to use K-means clustering to identify the ROIs. The ROIs was used for the subsequent step of source reconstruction. The motivation behind source reconstruction is to construct a PMI matrix and a PMI functional connectivity network at the level of the cortical based on the source signals. This will enable a clearer exploration of the cognitive differences between deception and honesty. Finally, this study builds a lie detection system based on the FCN classification algorithm. Each step is described in detail below:

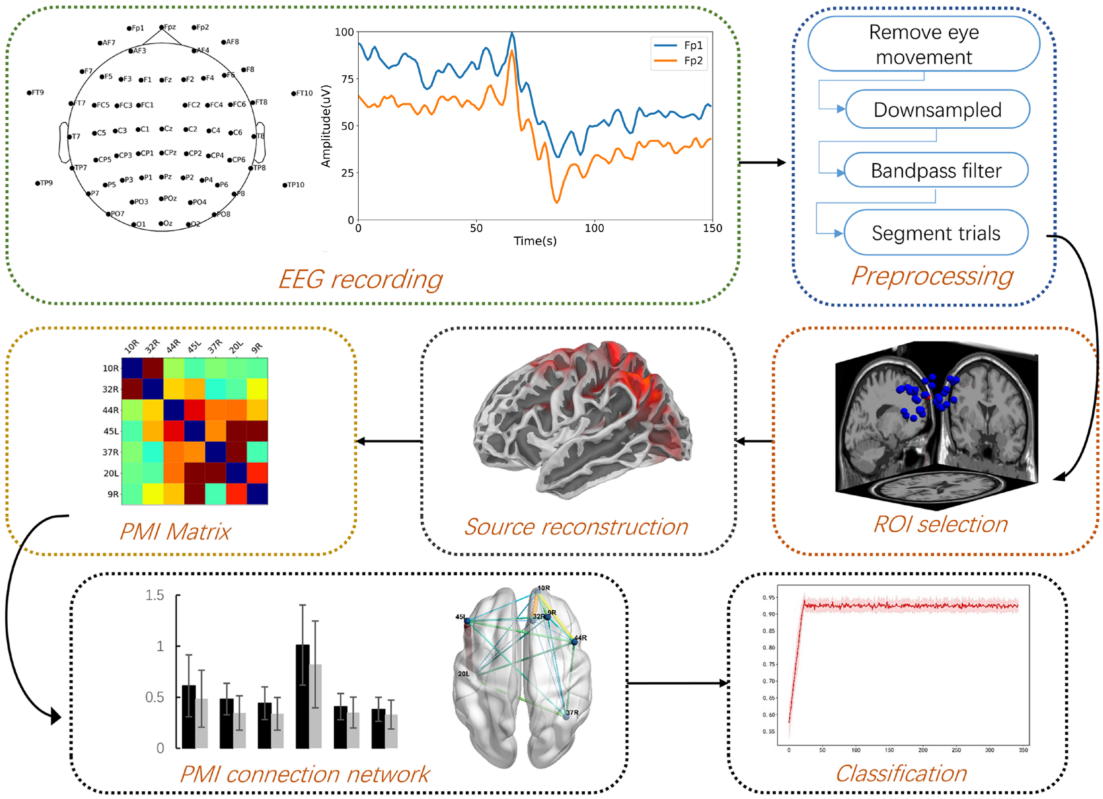

Figure 1. Flowchart of the proposed framework. The pipeline contains seven major steps: EEG recording, data preprocessing, ROI selection, source reconstruction, PMI matrix, PMI connection network, and FCN classification.

2.1. Participants

The present study received ethical approval from the Psychology Research Ethical Committee at South-Central MINZU University. A total of 36 right-handed, healthy college students were recruited as participants and provided informed consent prior to the experiment. The subjects were randomly assigned to either the lying group (9 males and 9 females, average age: 21.2 $\pm$ 1.2) or the innocent group (9 males and 9 females, average age: 21.3 $\pm$ 1.5). There were no significant differences in gender or age between the two groups. Participants were compensated for their participation following the experiment.

2.2. Experimental Protocol

This study utilized the standard Guilty Knowledge Test (GKT) paradigm, which involved presenting six items of jewelry along with their corresponding images as experimental stimuli. The set of jewelry images was presented to both the lying and innocent groups, the former group was instructed to "steal" one of the items from the set, while the latter one was not required to do so. The purpose of this was to simulate a real crime scenario. The specific experimental procedure is as follows:

Each participant in the lying group was instructed to open two safes, each containing a piece of jewelry. They were required to memorize the details of both pieces of jewelry and were instructed to randomly steal one of the jewels from the box. The stolen jewelry was designated as the probe stimulus (P), while the jewelry in the unselected safe was designated as the target stimulus (T). The remaining four stimuli were designated as irrelevant stimuli (I). In the innocent group, participants were required to randomly selected one of the two safes and observed the jewelry inside before returning it to its original safe. The jewelry in this safe was designated as the target stimulus (T), while the jewelry within the other safe was designated as the probe stimulus (P). The remaining four stimuli were labeled as irrelevant stimuli (I). After completing the preparations, each participant entered a quiet laboratory room with a constant temperature of 27 °C and sat in a chair to begin the experiment. The participants used a mouse with two buttons to respond. The left button indicated "No", indicating that the participant had seen the stimulus before the recording phase, while the right button indicated "Yes", indicating that they had not seen the stimulus before. During the experiment, the participants were asked to avoid any actions that could cause motion artifacts, such as chewing, swallowing, or blinking.

Figure 2 shows the schematic diagram of the experimental protocol. At the beginning of the experiment, a prompt marked with a "+" symbol was displayed on the screen for a duration ranging from 0.4 s to 0.6 s, after which the experimental stimuli were presented for 0.5 s. The participants were required to respond correctly and promptly to the experimental stimuli based on the task requirements. After the participants responded to the stimuli, the stimuli disappeared automatically and the reaction time was recorded. Subsequently, a post-rest period followed. The inter-stimulus interval was randomly varied between 1.6 s and 1.8 s. During the response period, guilty participants were required to press the left button when presented with the P stimulus, thereby deliberately hiding the fact that they stole the jewel. However, they honestly responded to the T and I stimuli. In contrast, innocent participants truthfully responded to all three types of stimuli.

The experiment consisted of three sessions, with each session comprising 180 trials (30 P, 30 T, and 120 I trials) lasting approximately 5 min. After each session, there was a 2 min rest period.

2.3. EEG Data Recording and Preprocessing

In this study, the EEG data were collected using the NeuroScan recording system (Compumedics Neuroscan, Charlotte, NC, USA) and a 64-channel cap arranged according to the 10-10 system. Horizontal and vertical electrooculography (EOG) electrodes were placed at the outer corner of the eye and under the left eye, respectively, approximately 2 cm below the eye. The EEG data were sampled at a frequency of 500 Hz, and the impedance of each electrode was kept below 5 KΩ. The data were preprocessed using MATLAB R2012b

(Mathworks Inc., Natick, MA, USA) and the EEGLAB toolbox. The data were first corrected for eye movement, using an autoregressive model provided by the NeuroScan system. Segments with severe saccades and electromyography (EMG) artifacts were then identified and removed from the data through visual inspection. The data were then downsampled to a frequency of 200 Hz and filtered using a 0.01–40 Hz bandpass filter. In this study, we focused on analyzing the signal of P stimuli, so the data were divided into epochs ranging from 300 milliseconds before to 1300 milliseconds after the onset of the P stimulus (−300 ms to 1300 ms, with a total duration of 1600 ms). The period from −300 ms to 0 ms served as the baseline for signal correction. To improve the signal-to-noise ratio of each participant's data, cross-trial averaging was used, with five trials per participant being averaged into a single epoch [44]. After preprocessing, 315 P stimulus trials were available for analysis in both the innocent and lying groups. The reduction in the number of P stimuli was due to the removal of artifactual segments in order to maintain consistency in the number of trials for both groups.

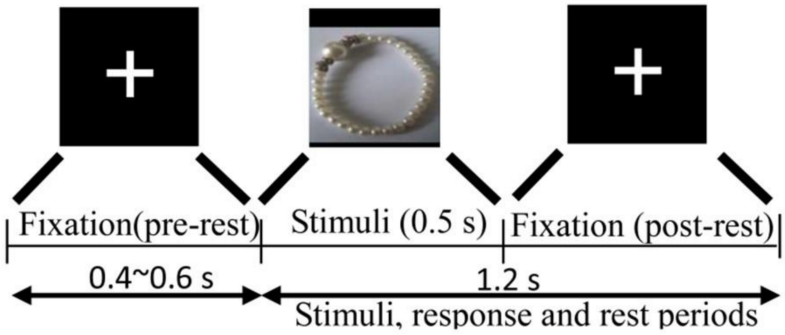

Figure 2. Schematic diagram of stimulus presentation in the experiment.

2.4. ROI Selection

To identify connectivity networks in the source space more accurately, we employed preprocessed data based on the lying group and utilized independent component analysis and K-means clustering to estimate regions of interest (ROIs). The specific method procedure was as follows: First, use the InfomaxICA algorithm in the EEGLAB toolbox to calculate the independent components (ICs) of the preprocessed EEG data of the lying group. The equivalent dipole positions of all ICs were then calculated using EEGLAB's DIPFIT2 plugin. Dipole positions, power spectra, and scalp maps of ICs with residual variance < 15% were concatenated as feature vectors and fed into the K-means algorithm for cluster analysis. Finally, the cluster centroids, defined by the results of K-means, were mapped to the corresponding Brodmann areas (BAs) using their Talairach coordinates. The BAs and corresponding Talairach coordinates are reported in the results. Additionally, these related BAs will be used as ROIs in the subsequent source reconstruction analysis.

2.5. Source Reconstruction

The aim of this section was to reconstruct the cortex source signal on the selected ROI in response to P stimulation in both groups of subjects. Various methods are developed for the solution of source reconstruction, including the minimum norm method (MN), low-resolution brain electromagnetic tomography (LORETA), and standardized LORETA, among others. In contrast to MN and LORETA, sLORETA performed source estimation based on the current density, which was parsed by the minimum norm solution and standardized by its variance. Therefore, the sLORETA method offers higher-quality results in terms of precise localization and zero-positioning error [42,43]. The details about sLORETA can be expressed as follows:

$$S_\phi = KJK^T + S_\varphi^{Noise} = KK^T + \alpha H \quad (1)$$

S_ϕ is the electrical potential variance. K is the lead field matrix. J is the variance of the source current density and S_φ^{Noise} is the variance of noise. The matrix H means the average reference operator and $\alpha \geq 0$ is the regularization parameter.

The variance of the estimated current density can be expressed as:

$$S_{\hat{J}} = TS_\phi T^T = T(KK^T + \alpha H)T^T = K^T[KK^T + \alpha H]^+ K \tag{2}$$

T is the inverse operator. Finally, the sLORETA method gives the estimate of standardized current density power, as follows:

$$\sigma_v = \left[S_{\hat{J}}\right]_v^{-\frac{1}{2}} \hat{j}_v \tag{3}$$

$$\sigma_v^T \sigma_v = j_v^T \left[S_{\hat{J}}\right]_v^{-1} \hat{j}_v \tag{4}$$

where $\left[S_{\hat{J}}\right]_v \in \mathbb{R}^{3\times 3}$ is the estimated current density value at the vth voxel obtained by the minimum norm estimation method, and $\left[S_{\hat{J}}\right]_v \in \mathbb{R}^{3\times 3}$ is the vth diagonal matrix in $S_{\hat{j}}$. In this paper, according to the data-driven approach in the previous step, the seven BAs were determined as ROIs before conducting the sLORETA analysis. We used the P stimulation trials from two groups of subjects as the input data for sLORETA analysis to estimate the current source density and, in turn, determine the cortex source signal in individual ROIs.

2.6. Partial Mutual Information

In order to solve the problem of pseudo-connected edges caused by the MI method, Frenzel introduced a new concept of partial independence and proposed a new measurement method, partial mutual information (PMI), to measure the non-linear direct correlation between two sequences. Consider two random variables: X and Y. If X and Y are independent random variables under the condition Z and the correlation between X and Y is zero, then it can be shown that:

$$p(x|z)p(y|z) = p(x, y|z) \tag{5}$$

The partial independence of random variables X and Y under the given condition Z is defined as:

$$p*(x|z)p*(y|z) = p(x, y|z) \tag{6}$$

where $p*(x|z)$ and $p*(y|z)$ are defined as:

$$p*(x|z) = \sum_y p(x|z, y)p(y) \tag{7}$$

$$p*(y|z) = \sum_x p(y|z, x)p(x) \tag{8}$$

According to the partial independence formula and Kullback–Leibler Divergence, *PMI* is defined as:

$$\begin{gathered} PMI(X, Y|Z) = \sum_{x,y,z} p(x, y, z) \log \frac{p(x,y|z)}{p^*(x|z)p^*(y|z)} \\ PMI(X, Y, Z) \geq 0 \end{gathered} \tag{9}$$

This formula expresses the direct correlation between signal variables X and Y. The larger the value, the stronger the correlation between the two. The *PMI* value is zero when X and Y are partially independent. When applied to the construction of the functional connection network of the brain regions, X and Y represent the neuroelectric signals of the two brain regions and the *PMI* directly reflects the intensity of the information flow

between the two brain regions. In this study, *X* and *Y* represent the selected ROIs used to compute the *PMI* values, while *Z* represents the set of other ROIs that were not chosen.

Based on the source data of the above two types of subjects, the *PMI* value between each ROI was calculated, and finally 630 *PMI* matrices (7×7) were generated. In this way, a brain network with ROI as the node and partial mutual information as the connecting edge was constructed. This work is focused on the analysis of the difference between each activated brain area when lying compared to the same brain area in the innocent group, which also provides the basic work for the next step of feature extraction.

2.7. Feature Extraction and Classification

The *t*-test was used to perform statistical analysis on the network connection edges of the two groups. Edges with significant differences were selected as classification features. To distinguish the features, the three-layer fully connected network (FCN) was designed as the classifier. FCN includes an input layer, an output layer, and multiple hidden layers connecting the input layer and the output layer. Here, the number of hidden layers is 1. K-fold cross-validation is used to evaluate the model. The data set was separated into k subsets, with k-1 subsets serving as the training set and the remaining k subset serving as the test set. The technique was performed k times to calculate the accuracy for each test set. The accuracy of our model was evaluated using a statistical 6-fold cross-validation technique in this work.

In previous research on lie detection using EEG, researchers have utilized the method of phase synchronization to develop a lie detection system. This involves applying functional connectivity indicators such as Phase Locking Value (PLV) and Phase Lag Index (PLI) to construct a feature vector. This feature vector is then sent to a machine-learning model for classification, which is used to build a polygraph system. At the same time, the Phase Lag Index (PLI) and Phase Locking Value (PLV) were used for comparative analysis.

3. Results

3.1. ROI Result

By applying independent component analysis and K-means clustering to the EEG data of the lying group, we were able to map the Talairach coordinates of each cluster's centroids to specific regions of the cerebral cortex. During the GKT task, we identified several brain areas of the lying group that were consistently activated, including the aPFC (BA10R), dACC (BA32R), IFG (BA44R), Broca's area (BA45R), FG (BA37R), IT (BA20L), and DLPFC (BA9R). A total of seven Brodmann areas were identified as regions of interest (ROI). The results of the clustering and corresponding brain area information are presented in Table 1.

Table 1. The size of the clusters and their corresponding brain regions and Talairach coordinates.

Component Clusters	Brain Regions	Talairach Coordinates			Cluster Size
		x	y	z	
1	Anterior prefrontal cortex (BA10R)	8	59	−11	18
2	Dorsal anterior cingulate cortex (BA32R)	4	−2	37	17
3	Inferior frontal gyrus (BA44R)	43	4	9	28
4	Broca-Triang (BA45R)	−56	17	2	28
5	Fusiform gyrus (BA37R)	62	−50	8	26
6	Inferior temporal gyrus (BA20L)	−58	−28	−17	33
7	Dorsolateral prefrontal cortex (BA9R)	21	45	34	25

3.2. Functional Connection Matrix and Statistical Analysis

The PMI adjacency matrix was built using the source signal. Figure 3 depicts the entire average PMI matrix of the lying and innocent groups. Each group received a total of 315 samples. The data were standardized and then graphed to visualize them clearly. It can be clearly observed that there are differences in some values of the two sets of PMI matrix values. The average PMI of the lying group is higher than that of the innocent group on some specific connection edges. The *t*-test were carried out separately for the PMI adjacency matrix's off-diagonal elements. The two data sets have been tested for normality and homogeneity of variances before the *t*-test, and met the normal distribution and homogeneity of variance. The difference was considered significant at $p < 0.05$. Figure 4 shows the six PMI connection pairs with significant differences after the one-sided *t*-test (lying > innocent), and the corresponding probability density function, mean ± SD. For visualization purposes, only partial scatter points are plotted and the distribution of scatter points that have been plotted is consistent with the corresponding probability density distribution.

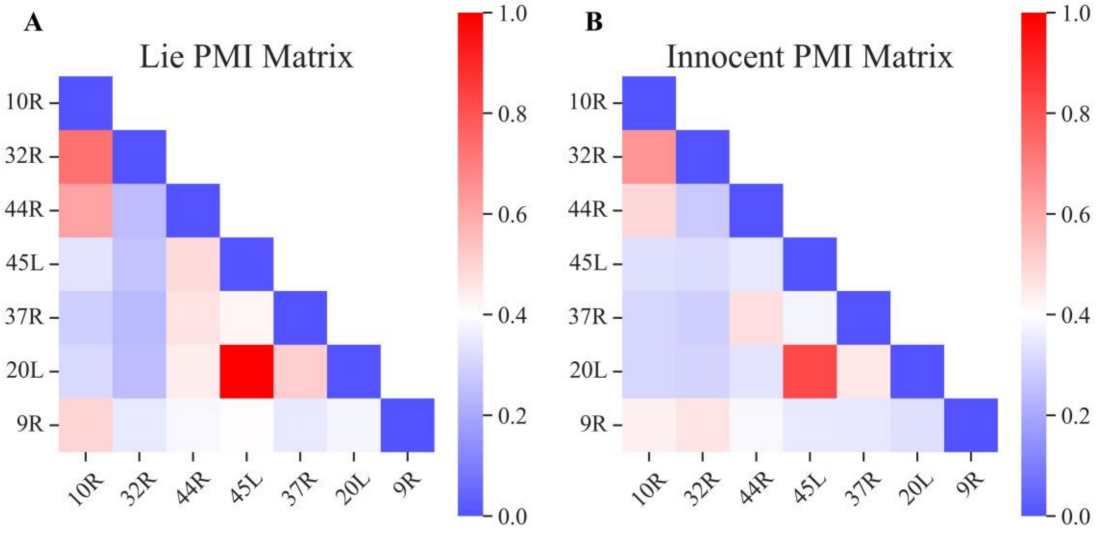

Figure 3. (**A**) The average PMI adjacency matrix of the lying group. (**B**) The average PMI adjacency matrix of the innocent group. The diagonal is conventionally set to 0 for all nodes. Only the lower half of the adjacency matrix is shown, which is due to PMI's symmetry.

3.3. Functional Connection Network Analysis

Considering the statistical results of connection edges, the topography of the PMI matrix for the innocent group (Figure 5A) and the lying group (Figure 5B) are shown below, respectively. For better visualization, only connection edges with PMI values greater than 0.4 have been drawn. Concerning the topography shown in Figure 5, the blue nodes represent the center points of each brain region obtained by the K-means algorithm, and the connection lines of different colors and thickness represent the connection strength of each brain area, which means the intensity of information exchange. Specifically, compared to the lying group, the distribution of strong connectivity values between ROIs in the innocent group is more sparse. The innocent group had six edges, and the lying group had ten edges. Moreover, in the lying group, there was a greater degree of information transfer between the left and right hemispheres of the brain. This was demonstrated by a higher distribution of functional connection values between hemispheres, including connections such as 20L-44R and 45L-44R, among others. In addition, Figure 5B depicts the topography of the difference matrix for comparison. Only connection edges with significant differences have been drawn. There are three functional connections from the frontal region to the frontal region (10R-44R, 45L-9R, 45L-44R), and three functional connections from the frontal region to the central region (45l-20L,9R-20L,44R-20L).

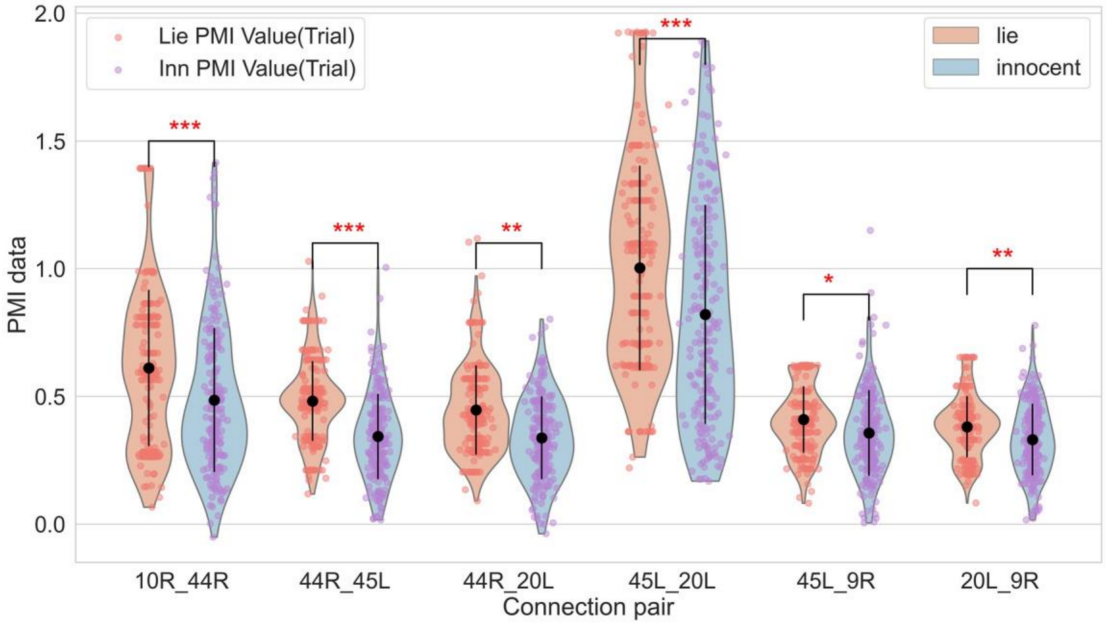

Figure 4. Six PMI connection pairs with significant differences between the lying and honest groups. A violin plot is utilized to depict the probability density distribution of PMI values for each connection pair among the two groups of subjects. Black dots and error bars indicate the means ± SD in each group, whereas colored dots indicate trial-level estimates (n = 100/315 trial). p values are indicated by stars: * $p < 0.05$, ** $p < 0.01$, and *** $p < 0.001$.

3.4. Classification Results

The six PMI connection edges with significant differences were used as features and sent to the FCN classifier for classification by six-fold cross-validation. We ended up with an average test accuracy of 88.5%. Based on the experimental data, this paper also used the phase-synchronization-based analytical methods PLI and PLV to calculate functional connectivity. Before computation, we performed the same feature extraction and classification process and compared it with the PMI classification accuracy results. The above results, shown in Table 2, indicate that the PMI method achieved the best performance and was extremely effective for differentiating lying from truth telling.

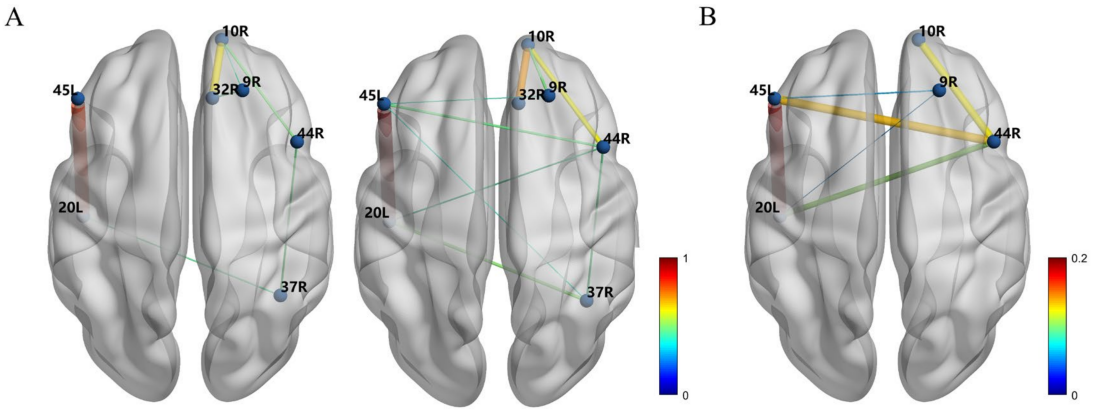

Figure 5. The topography of the PMI matrix results. (**A**) show the PMI topography in the innocent group and lying group. (**B**) represents the difference topography between the innocent group and the lying group (lying–innocent).

Table 2. Classification accuracy under different connectivity metrics.

Connectivity Metrics	Classification Accuracy (%)		
	Sensitivity	**Specificity**	**Balanced Accuracy**
PLV	65.2 ± 4.61	72.1 ± 3.83	70.7 ± 4.37
PLI	79.0 ± 5.54	68.3 ± 4.23	74.3 ± 3.91
PMI	92.4 ± 2.52	81.5 ± 4.26	88.5 ± 3.66

4. Discussion

In this study, EEG signals were collected and carefully preprocessed using the GKT paradigm. To analyze changes in the brain network during lying, the researchers employed a data-driven approach to identify the cortex source and used sLORETA to set regions of interest (ROIs). A PMI network was then constructed from the source signal and used as a feature for classification. A feature extraction step was performed, and a lie detection system was developed using a fully convolutional network (FCN) classifier. The results of this analysis are presented in the following findings:

This study found that brain regions activated during lying are primarily located in the frontal, parietal, and temporal lobes, as shown in Table 1, which are critical for the successful execution of deception. Previous research has consistently identified the involvement of the frontoparietal network in deception, and the medial temporal lobe (MTL) has been found to contribute to both working memory and long-term memory encoding [45]. The activation of the dorsolateral frontal cortex (DLPFC, including BA9) has also been commonly reported in deception studies [46–48] due to its roles in higher-level cognitive control, decision making, memory [49], and motor control [50]. The DLPFC has been shown to play a significant role in inhibiting honest responses and generating dishonest responses [51]. The parietal cortex has been linked to retrieving episodic memories [13], connecting new information with prior knowledge [15], and a range of integrated functions including episodic memory retrieval [52–54]. The precuneus, a part of the parietal cortex, has also been found to be involved in these processes [55].

The analysis presented in Figures 3–5 demonstrates that the intensity of information exchange between certain brain regions is higher in the lying group compared to the honest group, with the frontal and temporal lobes showing the most pronounced differences. There is a strong functional connection strength between the visual ventral pathway of the frontal lobe and the temporal lobe in the lying group (44R-20L, 45L-20L), which may indicate that the observation of crime-related picture stimuli leads to an impaired episodic memory of crime details and an increase in cognitive load. Previous research has suggested that telling the truth requires less conscious control and cognitive resources than lying, as the act of deception involves increased task complexity and cognitive demands such as attention, memory, and inhibition [56]. Jung's research suggests that individuals who are guilty may require a higher cognitive load to respond to stimuli due to increased attention and allocation of cognitive resources [57]. Other studies have found that enhanced communication between the 44R and 45L brain regions is associated with an increased working memory load during the act of lying [14,58]. The 44R region has been identified as a key "hub" in connectivity networks, potentially reflecting brain activity related to episodic memory and new information encoding [59]. The BA 9R/10R regions have been linked to strategic processes in memory recall, recognition, and various executive functions, and the BA44 region has been implicated in selective response suppression in go/no-go tasks [60]. The communication between the frontal association area and the motor language center (10R-44R, 9R-45L) observed in this study suggests that the lying group experiences a higher cognitive load during the process of information processing, decision-making, and judgment compared to the honest group.

In general, when people start to lie, they need to compete with and suppress honest responses in their brains. This process of competition and inhibition can cause liars to engage in more thinking and information exchanges in response to stimuli, potentially leading to

increased communication between various brain regions in liars. At the same time, because liars must switch between the two responses of lying and honesty, and ensure consistency and coherence in different expressions, maintaining this facade requires a higher cognitive load and increased psychological pressure, which can result in increased activation of certain brain areas that are associated with deception. Overall, understanding the neural mechanisms underlying lying can provide insights into the complex cognitive and emotional processes involved in deception, and help us identify potential markers of deception that can be used in various contexts, such as criminal investigations, psychological assessments, and lie detection.

5. Conclusions

Although there have been many studies on EEG polygraph technology at home and abroad, there are still many details of the cognitive process of lying that need to be explored. Additionally, the relationship between brain activity and behavior is complex, and it is not always possible to infer specific cognitive processes from changes in brain activity. In this paper, on the basis of tracing the source of EEG signals, a cortical brain function network was constructed through PMI and the synergistic effect of various brain regions in the process of lying was studied. Detecting its direction loses causal information about the flow of information. Therefore, in the later stage, we will further characterize the activity of brain regions by constructing directional effect connections, so as to further study the cognitive activity mechanisms in the process of lying.

Author Contributions: F.L. wrote part of the manuscript and proposed the study. Q.K. simulated it, wrote part of the manuscript, reviewed and edited. J.G. made writing suggestions and reviewed and analyzed the proposed research. All authors have read and agreed to the published version of the manuscript.

Funding: This work was supported by the National Natural Science Foundation of China under Grant No. 61773408.

Institutional Review Board Statement: The study was conducted in accordance with the Declaration of Helsinki, and approved by the Psychology Research Ethical Committee at South-Central MINZU University (2021-SCUEC-016, 7 September 2021).

Informed Consent Statement: Informed consent was obtained from all subjects involved in the study.

Data Availability Statement: The data presented in this study are available on request from the corresponding author.

Conflicts of Interest: The authors declare no conflict of interest.

References

1. DePaulo, B.M.; Lindsay, J.J.; Malone, B.E.; Muhlenbruck, L.; Charlton, K.; Cooper, H. Cues to deception. *Psychol. Bull.* **2003**, *129*, 74. [CrossRef] [PubMed]
2. Vicianova, M. Historical Techniques of Lie Detection. *Eur. J. Psychol.* **2015**, *11*, 522–534. [CrossRef] [PubMed]
3. Grubin, D.; Madsen, L. Lie detection and the polygraph: A historical review. *J. Forensic Psychiatry Psychol.* **2005**, *16*, 357–369. [CrossRef]
4. Synnott, J.; Dietzel, D.; Ioannou, M. A review of the polygraph: History, methodology and current status. *Crime Psychol. Rev.* **2015**, *1*, 59–83. [CrossRef]
5. Farwell, L.A. Brain fingerprinting: A comprehensive tutorial review of detection of concealed information with event-related brain potentials. *Cogn. Neurodyn.* **2012**, *6*, 115–154. [CrossRef]
6. Petoft, A. An Overview of the Technical Limitations of Applying the fMRI Method in Neurolaw. *Bioeth. J.* **2020**, *9*, 95–107. [CrossRef]
7. Bai, X.; Zhang, P.; Zhang, Q.; Song, L.; Yang, Y. Applications of functional near-infrared spectroscopy to lying researches. *Adv. Psychol. Sci.* **2019**, *27*, 160–170. [CrossRef]
8. Abootalebi, V.; Moradi, M.H.; Khalilzadeh, M.A. A new approach for EEG feature extraction in P300-based lie detection. *Comput. Methods Programs Biomed.* **2009**, *94*, 48–57. [CrossRef]

9. Gao, J.; Yan, X.; Sun, J.; Zheng, C. Denoised P300 and machine learning-based concealed information test method. *Comput. Methods Programs Biomed.* **2011**, *104*, 410–417. [CrossRef]
10. Leue, A.; Lange, S.; Beauducel, A. "Have you ever seen this face?"—Individual differences and event-related potentials during deception. *Front. Psychol.* **2012**, *3*, 570. [CrossRef]
11. Abe, N. How the brain shapes deception: An integrated review of the literature. *Neuroscientist* **2011**, *17*, 560–574. [CrossRef]
12. Wang, H.; Chang, W.; Zhang, C. Functional brain network and multichannel analysis for the P300-based brain computer interface system of lying detection. *Expert Syst. Appl.* **2016**, *53*, 117–128. [CrossRef]
13. Wang, Y.; Ng, W.C.; Ng, K.S.; Yu, K.; Wu, T.; Li, X. An Electroencephalography Network and Connectivity Analysis for Deception in Instructed Lying Tasks. *PLoS ONE* **2015**, *10*, e0116522. [CrossRef]
14. Gao, J.-F.; Yang, Y.; Huang, W.-T.; Lin, P.; Ge, S.; Zheng, H.-M.; Gu, L.-Y.; Zhou, H.; Li, C.-H.; Rao, N.-N. Exploring time- and frequency-dependent functional connectivity and brain networks during deception with single-trial event-related potentials. *Sci. Rep.* **2016**, *6*, 37065. [CrossRef]
15. Gao, J.; Gu, L.; Min, X.; Lin, P.; Li, C.; Zhang, Q.; Rao, N. Brain Fingerprinting and Lie Detection: A Study of Dynamic Functional Connectivity Patterns of Deception Using EEG Phase Synchrony Analysis. *IEEE J. Biomed. Health Inform.* **2021**, *26*, 600–613. [CrossRef]
16. Bonita, J.D.; Ambolode, L.C.C.; Rosenberg, B.M.; Cellucci, C.J.; Watanabe, T.A.A.; Rapp, P.E.; Albano, A.M. Time domain measures of inter-channel EEG correlations: A comparison of linear, nonparametric and nonlinear measures. *Cogn. Neurodyn.* **2013**, *8*, 1–15. [CrossRef]
17. Schoffelen, J.-M.; Gross, J. Source connectivity analysis with MEG and EEG. *Hum. Brain Mapp.* **2009**, *30*, 1857–1865. [CrossRef]
18. Peng, S.-Y.; Zhou, D.; Zhang, J.-Q.; Wang, Y.; Gao, J.-F. Research on Mutual Information-Based Brain Network and Lie Detection. *Acta Electron. Sin.* **2019**, *47*, 1551–1556.
19. Singh, A.; Lesica, N.A. Incremental Mutual Information: A New Method for Characterizing the Strength and Dynamics of Connections in Neuronal Circuits. *PLoS Comput. Biol.* **2010**, *6*, e1001035. [CrossRef]
20. Frenzel, S.; Pompe, B. Partial Mutual Information for Coupling Analysis of Multivariate Time Series. *Phys. Rev. Lett.* **2007**, *99*, 204101. [CrossRef]
21. Niso, G.; Bruña, R.; Pereda, E.; Gutiérrez, R.; Bajo, R.; Maestú, F.; Del-Pozo, F. HERMES: Towards an Integrated Toolbox to Characterize Functional and Effective Brain Connectivity. *Neuroinformatics* **2013**, *11*, 405–434. [CrossRef] [PubMed]
22. Masuda, N.; Sakaki, M.; Ezaki, T.; Watanabe, T. Clustering Coefficients for Correlation Networks. *Front. Neuroinform.* **2018**, *12*, 7. [CrossRef] [PubMed]
23. Zhao, J.; Zhou, Y.; Zhang, X.; Chen, L. Part mutual information for quantifying direct associations in networks. *Proc. Natl. Acad. Sci. USA* **2016**, *113*, 5130–5135. [CrossRef] [PubMed]
24. Lai, M.; Demuru, M.; Hillebrand, A.; Fraschini, M. A comparison between scalp- and source-reconstructed EEG networks. *Sci. Rep.* **2018**, *8*, 12269. [CrossRef]
25. Luo, C.; Li, F.; Li, P.; Yi, C.; Li, C.; Tao, Q.; Zhang, X.; Si, Y.; Yao, D.; Yin, G.; et al. A survey of brain network analysis by electroencephalographic signals. *Cogn. Neurodyn.* **2021**, *16*, 17–41. [CrossRef]
26. Papadopoulou, M.; Friston, K.; Marinazzo, D. Estimating Directed Connectivity from Cortical Recordings and Reconstructed Sources. *Brain Topogr.* **2019**, *32*, 741–752. [CrossRef]
27. He, B.; Yang, L.; Wilke, C.; Yuan, H. Electrophysiological Imaging of Brain Activity and Connectivity—Challenges and Opportunities. *IEEE Trans. Biomed. Eng.* **2011**, *58*, 1918–1931. [CrossRef]
28. Li, F.; Yi, C.; Jiang, Y.; Liao, Y.; Si, Y.; Yao, D.; Zhang, Y.; Xu, P. The Construction of Large-Scale Cortical Networks for P300 From Scalp EEG. *IEEE Access* **2018**, *6*, 68498–68506. [CrossRef]
29. Kouti, M.; Ansari-Asl, K.; Namjoo, E. Emotion discrimination using source connectivity analysis based on dynamic ROI identification. *Biomed. Signal Process. Control* **2022**, *72*, 103332. [CrossRef]
30. Barzegaran, E.; Knyazeva, M.G. Functional connectivity analysis in EEG source space: The choice of method. *PLoS ONE* **2017**, *12*, e0181105. [CrossRef]
31. Rubega, M.; Carboni, M.; Seeber, M.; Pascucci, D.; Tourbier, S.; Toscano, G.; Van Mierlo, P.; Hagmann, P.; Plomp, G.; Vulliemoz, S.; et al. Estimating EEG Source Dipole Orientation Based on Singular-value Decomposition for Connectivity Analysis. *Brain Topogr.* **2019**, *32*, 704–719. [CrossRef]
32. Pascual-Marqui, R.D. Standardized low-resolution brain electromagnetic tomography (sLORETA): Technical details. *Methods Find. Exp. Clin. Pharmacol.* **2002**, *24* (Suppl. D), 5–12.
33. Jatoi, M.A.; Kamel, N.; Malik, A.S.; Faye, I.; Begum, T. A survey of methods used for source localization using EEG signals. *Biomed. Signal Process. Control* **2014**, *11*, 42–52. [CrossRef]
34. Padilla-Buritica, J.I.; Martinez-Vargas, J.D.; Castellanos-Dominguez, G. Emotion Discrimination Using Spatially Compact Regions of Interest Extracted from Imaging EEG Activity. *Front. Comput. Neurosci.* **2016**, *10*, 55. [CrossRef]
35. Lancaster, J.L.; Woldorff, M.G.; Parsons, L.M.; Liotti, M.; Freitas, C.S.; Rainey, L.; Kochunov, P.V.; Nickerson, D.; Mikiten, S.A.; Fox, P.T. Automated Talairach atlas labels for functional brain mapping. *Hum. Brain Mapp.* **2000**, *10*, 120–131. [CrossRef]
36. Courellis, H.; Mullen, T.; Poizner, H.; Cauwenberghs, G.; Iversen, J.R. EEG-Based Quantification of Cortical Current Density and Dynamic Causal Connectivity Generalized across Subjects Performing BCI-Monitored Cognitive Tasks. *Front. Neurosci.* **2017**, *11*, 180. [CrossRef]

37. Chikara, R.K.; Ko, L.-W. Modulation of the Visual to Auditory Human Inhibitory Brain Network: An EEG Dipole Source Localization Study. *Brain Sci.* **2019**, *9*, 216. [CrossRef]
38. Lachaux, J.; Rodriguez, E.; Martinerie, J.; Varela, F.J. Measuring phase synchrony in brain signals. *Hum. Brain Mapp.* **1999**, *8*, 194–208. [CrossRef]
39. Stam, C.J.; Nolte, G.; Daffertshofer, A. Phase lag index: Assessment of functional connectivity from multi channel EEG and MEG with diminished bias from common sources. *Hum. Brain Mapp.* **2007**, *28*, 1178–1193. [CrossRef]
40. Xiong, Y.; Gu, L.; Gao, J. Phase synchrony and its application to lie detection. In *Proceedings of the 2020 IEEE International Conference on Power, Intelligent Computing and Systems (ICPICS), Shenyang, China, 28–30 July 2020*; IEEE: Piscataway, NJ, USA, 2020; pp. 726–729. [CrossRef]
41. Si, H.F.; Xie, T.; Gao, J.F.; Guan, J.A.; Xiang, Z.Z.; Lan, C.Y.; Qing, X.H. Research on brain functional network and lie detection based on phase lag index. *Acta Electron. Sin.* **2018**, *46*, 1742.
42. Battista, F.; Otgaar, H.; Mangiulli, I.; Curci, A. The role of executive functions in the effects of lying on memory. *Acta Psychol.* **2021**, *215*, 103295. [CrossRef]
43. Gombos, V.A. The Cognition of Deception: The Role of Executive Processes in Producing Lies. *Genet. Social, Gen. Psychol. Monogr.* **2006**, *132*, 197–214. [CrossRef]
44. Mouraux, A.; Iannetti, G. Across-trial averaging of event-related EEG responses and beyond. *Magn. Reson. Imaging* **2008**, *26*, 1041–1054. [CrossRef] [PubMed]
45. Axmacher, N.; Schmitz, D.P.; Weinreich, I.; Elger, C.E.; Fell, J. Interaction of Working Memory and Long-Term Memory in the Medial Temporal Lobe. *Cereb. Cortex* **2008**, *18*, 2868–2878. [CrossRef] [PubMed]
46. Nuñez, J.M.; Casey, B.; Egner, T.; Hare, T.; Hirsch, J. Intentional false responding shares neural substrates with response conflict and cognitive control. *Neuroimage* **2005**, *25*, 267–277. [CrossRef] [PubMed]
47. Karim, A.A.; Schneider, M.; Lotze, M.; Veit, R.; Sauseng, P.; Braun, C.; Birbaumer, N. The Truth about Lying: Inhibition of the Anterior Prefrontal Cortex Improves Deceptive Behavior. *Cereb. Cortex* **2010**, *20*, 205–213. [CrossRef]
48. Ganis, G.; Kosslyn, S.; Stose, S.; Thompson, W.; Yurgelun-Todd, D. Neural correlates of different types of deception: An fMRI investigation. *Cereb. Cortex* **2003**, *13*, 830–836. [CrossRef]
49. Christ, S.E.; Van Essen, D.C.; Watson, J.M.; Brubaker, L.E.; McDermott, K.B. The Contributions of Prefrontal Cortex and Executive Control to Deception: Evidence from Activation Likelihood Estimate Meta-analyses. *Cereb. Cortex* **2009**, *19*, 1557–1566. [CrossRef]
50. Leung, H.-C.; Gore, J.C.; Goldman-Rakic, P.S. Sustained Mnemonic Response in the Human Middle Frontal Gyrus during On-Line Storage of Spatial Memoranda. *J. Cogn. Neurosci.* **2002**, *14*, 659–671. [CrossRef]
51. Ito, A.; Abe, N.; Fujii, T.; Ueno, A.; Koseki, Y.; Hashimoto, R.; Mugikura, S.; Takahashi, S.; Mori, E. The role of the dorsolateral prefrontal cortex in deception when remembering neutral and emotional events. *Neurosci. Res.* **2011**, *69*, 121–128. [CrossRef]
52. Cabeza, R.; Ciaramelli, E.; Olson, I.R.; Moscovitch, M. The parietal cortex and episodic memory: An attentional account. *Nat. Rev. Neurosci.* **2008**, *9*, 613–625. [CrossRef]
53. Cabeza, R.; Nyberg, L. Imaging Cognition II: An Empirical Review of 275 PET and fMRI Studies. *J. Cogn. Neurosci.* **2000**, *12*, 1–47. [CrossRef]
54. Lou, H.C.; Luber, B.; Crupain, M.; Keenan, J.P.; Nowak, M.; Kjaer, T.W.; Sackeim, H.A.; Lisanby, S.H. Parietal cortex and representation of the mental Self. *Proc. Natl. Acad. Sci. USA* **2004**, *101*, 6827–6832. [CrossRef]
55. Bruner, E.; Rangel de Lazaro, G.; de la Cuétara, J.M.; Martín-Loeches, M.; Colom, R.; Jacobs, H.I. Midsagittal brain variation and MRI shape analysis of the precuneus in adult individuals. *J. Anat.* **2014**, *224*, 367–376. [CrossRef]
56. Neubauer, A.C.; Sange, G.; Pfurtscheller, G. Psychometric intelligence and event-related desynchronization during performance of a letter matching task. In *Event-Related Desynchronization. Handbook of Electroencephalography and Clinical Neurophysiology*; Elsevier BV: Amsterdam, The Netherlands, 1999; pp. 219–231.
57. Jung, E.K.; Kang, K.-Y.; Kim, Y.Y. Frontoparietal activity during deceptive responses in the P300-based guilty knowledge test: An sLORETA study. *Neuroimage* **2013**, *78*, 305–315. [CrossRef]
58. Kohan, M.D.; Nasrabadi, A.M.; Sharifi, A.; Shamsollahi, M.B. Interview based connectivity analysis of EEG in order to detect deception. *Med. Hypotheses* **2020**, *136*, 109517. [CrossRef]
59. Gao, J.; Min, X.; Kang, Q.; Si, H.; Zhan, H.; Manyande, A.; Tian, X.; Dong, Y.; Zheng, H.; Song, J. Effective connectivity in cortical networks during deception: A lie detection study using EEG. *IEEE J. Biomed. Health Inform.* **2022**, *26*, 3755–3766. [CrossRef]
60. Ullsperger, M.; Fischer, A.G.; Nigbur, R.; Endrass, T. Neural mechanisms and temporal dynamics of performance monitoring. *Trends Cogn. Sci.* **2014**, *18*, 259–267. [CrossRef]